Mechanism of UV Photoreactivity of Alkylsiloxane Self-Assembled Monolayers

Tao Ye, Eric A. McArthur, and Eric Borguet*

Department of Chemistry, Temple University, Philadelphia, Pennsylvania 19122

Received: June 14, 2004; In Final Form: September 23, 2004

A molecular level understanding of the photoreactivity of self-assembled monolayers (SAMs) becomes increasingly important as the spatial resolution starts to be limited by the size of the resist and the spatial extent of the photochemical reactions in photoresist micropatterning. To this end, a number of surface characterization techniques were combined to understand the reactive agents, reactive sites, kinetics, and reaction pathways in the UV photoreactivity of octadecylsiloxane (ODS) SAMs. Quantitative analysis of our results provides evidence that ground state atomic oxygen is the primary reactive agent for the UV degradation of ODS SAMs. UV degradation, which follows zero-order kinetics, results in the scission of alkyl chains instead of the siloxane headgroups. Our results suggest that the top of the ODS SAMs is the preferential reactive site. Using a novel, highly surface sensitive technique, fluorescence labeling of surface species, we identified the presence of submonolayer quantities chemical functional groups formed by the UV degradation. These groups are intermediates in a proposed mechanism based on hydrogen abstraction.

1. Introduction

There has been intense interest in the growth of self-assembled monolayers (SAMs).[1] In contrast, much less attention has been paid to the reactivity of SAMs. The stability of SAMs is a prerequisite in their technological applications. Alkanethiol SAMs have been found to have lifetimes ranging from hours to months in ambient environment[2] and degrade in minutes under ultraviolet (UV) irradiation.[3] The reactivity of alkanethiol SAMs has been attributed to the thiolate headgroups, which are prone to oxidation.[3] Even the alkyl chains can degrade under harsh conditions, e.g., under photo or electron irradiation.[4–6] Knowledge of SAM photoreactivity may help to design and prepare more stable SAMs for technological applications.

While we need to improve the stability of SAMs, controlled reactions of SAMs can be desirable in some cases. Photoreactivity of SAMs can be exploited to selectively modify SAMs for various applications. Understanding the photoreactivity of SAMs is important for optimizing photoresist patterning processes involving SAMs.[7–11] As the feature sizes in lithography continue to scale down, there is an increasing demand on the resist films in terms of thickness and structural uniformity.[12–15] SAMs are an attractive candidate for nanoscale resists due to their molecular thickness and well-defined structure on nanometer length scales, which in principle should enable nanometer resolution in pattern transfer. In addition, photomodification of SAMs may serve as a convenient route to attach functional groups to SAMs, enabling one to tailor wettability, adhesion, and electrical properties of the monolayers.[16]

On a more fundamental level, their molecularly well-defined structures render SAMs a model system to probe the relationship between structure and photoreactivity in condensed phases, which has implications from organic aerosol chemistry to photoresist micropatterning.[17–21] A molecular level understanding of how the photoresist reacts will be increasingly important in high-resolution photoresist micropatterning since the resolu-

tion may begin to be limited by the size of the resist and spatial extent of the photochemical reactions, as the feature sizes approach nanometer scales.[22] The mechanisms of photooxidation of organic materials in the condensed phase is much more complex than in the gas phase.[19,23] SAMs afford the opportunity to systematically vary the structure and composition of organic layers to understand from a molecular level how these factors affect the reactivity.

1.1. Possible Mechanisms of Photoreactivity of SAMs. Depending on the wavelength, the nature of the functional groups in the SAMs, the substrate, and the ambient environment, photons can modify the SAMs with different mechanisms. We attempt to categorize the mechanisms according to the active agents involved.

1.1.1. Direct Photodissociation. Photons can be directly responsible for the dissociation of the organic molecules in SAMs. UV photons in resonance with electronic transitions in unsaturated SAM layers (such as a π–π^* transition) can induce photolysis.[7] However, direct photolysis of saturated alkyl SAMs requires a σ–σ^* transition of C–H or C–C bonds induced by absorption of photons with wavelength less than 160 nm.[24]

1.1.2. Electron Mediated. Photons can ionize the underlying substrate or the monolayer, which leads to further chemical transformation and dissociation. X-ray induced modification of SAMs is believed to proceed via this mechanism.[25–27] Although there is little absorption of X-rays by organic monolayers, photoelectrons generated from the substrate can interact with the organic monolayers. Indeed, the damage of SAMs by X-ray degradation[26] is remarkably similar to the electron damage of SAMs.[28] Both involve dehydrogenation and cross-linking of the alkyl chains. Both mechanisms result in very little loss of carbon content. Both mechanisms result in incorporation of oxygenated functional groups upon exposure to air. It is believed that electron impact induces C–H and C–C bond scission, forming radicals.[28] The radicals can undergo cross-linking and oxygenation.[28] Recently, Uosaki and co-workers found that UV irradiation of an alkyl monolayer covalently attached to Si(111) results in the cleavage of the headgroups (Si–C), suggesting

* To whom correspondence should be addressed. E-mail: eborguet@temple.edu.

the role of photoelectrons.[29] The energy of photoelectrons generated by UV is only about a few eVs. The underlying mechanism (whether it is electron- or hole-mediated, whether the charges can reside on the Si−C long enough to induce bond cleavage or not) has yet to be understood.[29]

1.1.3. Chemical Reactant Mediated. In an ambient environment, UV light may generate highly oxidative species, such as ozone, atomic oxygen, and hydroxyl radicals.[30] The reactive species may subsequently react with the monolayers. A number of studies have attributed the primary degradation pathway of alkanethiol SAMs in ambient and under low UV intensity (μW/cm^2 to mW/cm^2) to ozonolysis.[2,3,31−33] In this mechanism, it is suggested that photogenerated ozone attacks the thiolate headgroups to produce solvent-labile species and cleavage of the C−S bond. In contrast, UV photooxidation of alkylsiloxane SAMs has been attributed to the reaction between hydrocarbon chains and atomic oxygen or other oxygen-containing radicals.[34,35]

It should be noted that the photoreactivity of SAMs may involve more than one mechanism at the same time. For example, X-ray degradation of SAMs is initiated by electrons, but subsequently chemical reactants may participate in the degradation as well.[26]

1.2. Objectives of This Study. Although it is well-known that many SAMs degrade under UV irradiation, and this has been utilized to pattern SAMs,[8] the reactive species, the reactive sites, the resulting nanoscale and the reaction mechanism remain unclear. For example, it is unclear whether the degradation of alkylsiloxane SAMs proceeds via direct photodissociation of alkyl chains,[8] or oxidation by reactive species generated by UV light under ambient.[34] The precise roles of the headgroups and the alkyl chains in the degradation remain poorly understood. In our previous report, we presented evidence that ozone is not the active agent in alkylsiloxane SAM degradation under UV illumination in air.[30] A combination of UV and oxygen is necessary for monolayer degradation to proceed. AFM measurements on submonolayer coverage SAMs suggested that the coverage of SAM islands did not change after UV irradiation, although the height of the islands was reduced, suggesting the lack of a role of defects in the degradation process.[30] This was in stark contrast to the case of alkanethiols, where structural defects in the SAM were shown to be necessary for ozonolysis.[2] We suggested that the hydrocarbon chains, instead of headgroups, are the reactive sites under UV irradiation in ambient.[30]

In the present report, we performed a more detailed investigation to achieve a molecular scale understanding of UV photoreactivity of ODS SAMs. We provide quantitative evidence that atomic oxygen is the primary agent for the UV degradation of ODS SAMs. UV degradation results in the scission of alkyl chains instead of the siloxane headgroups. The zeroth-order kinetics we observed implies that the chains are cut in a top-down fashion, consistent with our previous AFM results that indicated no coverage change of ODS islands after UV irradiation.[30] We found that degradation introduces microscopic roughness to ODS SAMs as suggested by FT-IR and contact angle results. Using a novel, highly surface sensitive technique, fluorescence labeling of surface species (FLOSS), we identified the presence of submonolayer quantities of chemical functional groups formed by the UV degradation. This identification of intermediates allows a probable reaction mechanism to be identified. Such understandings on the reactivity of SAMs have implications in high-resolution photopatterning of molecular scale resists.
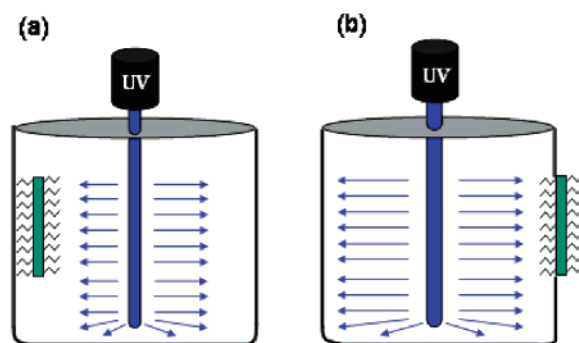

Figure 1. UV chamber (a) Irradiation configuration 1, where both sides of the sample are exposed to the chamber. (b) Irradiation configuration 2, where only a single side is exposed to the reactive species produced in the chamber.

2. Experimental Section

2.1. SAM Preparation. Microscope glass slides (VWR Scientific, cat. no. 48300-025) and native SiO$_2$ grown on Si wafers were used as the substrates. The substrates were sonicated in acetone, methanol, and then water. The substrates were then subjected to cleaning in a UV/ozone chamber 1 h or to RCA SC1 H$_2$O:NH$_4$OH:30%H$_2$O$_2$ (4:1:1) treatment at 80−90 °C for 30 min to 1 h. After final treatment, the substrates have a water contact angle close to 0°, suggesting that both UV/ozone and RCA SC1 treatment are effective in producing clean and hydrophilic surfaces.

The cleaned substrates were then immersed in millimolar OTS solutions prepared in a mixture of hexadecane (99%, Acros), HCCl$_3$ (GR grade, EM Science), and CCl$_4$ (GR grade EM Science) in 10/1.5/1 volumetric ratio or millimolar OTS toluene solution for about 1 h.[36−38] After reaction, the samples were rinsed in HCCl$_3$ at least three times.

2.2. UV Irradiation. The ODS-covered samples were irradiated in a homemade Pyrex glass UV chamber with a low-pressure Hg/Ar lamp (Oriel Instruments) with total intensity of ∼2 mW/cm^2 at a working distance of 3 cm (Figure 1). The primary wavelength of the lamp is 254 nm. The UV light at 183 nm, albeit constituting only 3% of the total intensity, is responsible for the ozone generation.[33] Before placing the sample in the UV chamber, the UV lamp was powered on for at least 15 min to allow it to reach a stable intensity and for a steady-state ozone concentration to build up in the chamber.[31] The ozone concentration was determined by a direct photometric method.[39] The ozone generated in the chamber was captured in a 1-cm path length quartz cuvette. Assuming an absorption cross section of 1150×10^{-20} cm^2 at 255 nm, the UV absorbance was used to calculate the concentration.[40] The steady-state concentration of ozone in the UV chamber was found to be 100 ± 10 ppm.

2.3. Sample Characterization. 2.3.1. Water Contact Angle. Unirradiated SAMs were cleaned with acetone or chloroform prior to characterization. Unless otherwise mentioned, irradiated SAMs were characterized without any treatment because perturbations induced by rinsing are a concern for the irradiated samples. Water contact angle measurements were performed using the sessile drop method with VCA-2000 Laboratory Surface Analysis system (AST Productions Inc). Static contact angles were measured. Four to five measurements were averaged for each sample.

2.3.2. FT-IR Measurements. Transmission FT-IR spectra were collected with Nicolet Avatar 360 IR or a Brüker Tensor 27 FTIR spectrometer at normal incidence. Spectral resolution was either 4 or 8 cm^{-1}. 256 to 512 scans were averaged. Most

Photoreactivity of Alkylsiloxane Monolayers

J. Phys. Chem. B, Vol. 109, No. 20, 2005 **9929**

FT-IR spectra were obtained from SAMs supported on glass slides. Samples for FT-IR are irradiated in configuration b in Figure 1, by exposing one side to the UV for the desired amount of time and then exposing the other side to the UV for an equal amount of time. Corresponding uncoated substrates were used as the background. The only exceptions were the FT-IR measurements in the carbonyl stretch region, performed on SAMs supported on oxidized silicon substrates. In that case, the background was N_2 instead of a cleaned substrate.

2.3.3. XPS Measurements. X-ray photoelectron spectra were obtained on a Physical Electronics model 550 apparatus, equipped with a cylindrical, double-pass analyzer. The front of the analyzer was apertured to restrict the acceptance angle to $\pm 6°$. The energy resolution of the apparatus was determined to be 1 eV. X-ray photoelectron spectra were taken using an Al $K\alpha$ X-ray source (1486.3 eV), and all the spectra were taken at a 30° takeoff angle. The pressure in the analytical chamber was $\sim 10^{-9}$ Torr during analysis. Spectra in the C(1s) (binding energy: 280−292 eV) region were collected.

2.3.4. Fluorescence Labeling of Surface Species (FLOSS). Chromophore labeling: micromolar solutions were prepared of either triphenylmethyl chloride (98%, Aldrich) in dimethylformamide (DMF, ACS grade, Baker), 1-pyrenemethylamine (95%, Aldrich) in ethanol (ACS grade, Pharmaco) or 1-naphthaleneethanol (99%, Aldrich) in methylenechloride (ACS grade, Fisher). The trityl and pyrene labeling reactions were carried out at room temperature for 2 h. The naphthalene labeling reaction was refluxed for 2 h with a catalytic amount of hydrochloric acid (CMOS grade, Baker). Fluorescence measurements were performed on a Jobin Yvon Horiba Spex Fluorolog 3 with 5-nm band-pass and five scan averages with samples situated at a 45° incident angle. Excitation and emission monochromators are double grating and detection is accomplished using a photo multiplier tube. Fluorescent signals for all samples were corrected for lamp fluctuations by recording the ratio of the fluorescence signal to a source reference photodiode.

Postreaction cleaning procedure: Following the chromophore grafting, sample surfaces (oxidized Si substrate) were rinsed with neat solvent. The samples were then sonicated in successively less polar solvents (methanol or acetone, then CH_2Cl_2, and finally hexane) to remove residual reactant species from the surface.

The calibration sample was marked with a diamond scribe defining the boundaries of the spot (4×6 mm) illuminated by the fluorometer. This facilitated realignment of the sample and ensured that the solution spread only in the defined area. A 5 μL drop of dilute solution was placed on the marked area of the sample and the solvent was allowed to evaporate.

Hydrolysis: To remove amino-pyrene covalently attached to SAMs, the samples are soaked in DI water containing a catalytic amount of mineral acid for ~ 1 h. The samples were then rinsed in successively less polar solvents (methanol or acetone, then CH_2Cl_2, and finally hexane).

3. Results

3.1. Contact Angle Results. The ODS SAMs are known to be remarkably stable in ambient over extended periods of time. There was no measurable change in the contact angles of the monolayers stored under ambient in our laboratory over several months. The contact angle of SAMs dropped significantly following a few minutes of UV irradiation in air. The increasing hydrophilicity of the surface can be explained by conversion of alkyl chains to hydrophilic groups, e.g., OH, aldehydes, or
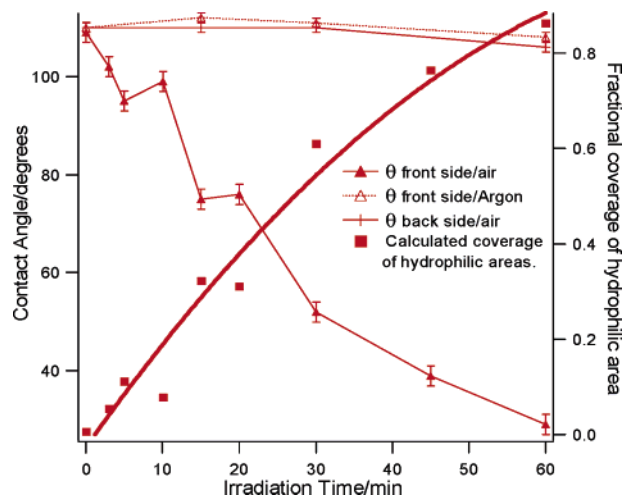

Figure 2. Contact angles of irradiated ODS SAMs on glass as a function of time under different ambient environments and effective fractional coverage of hydrophilic groups calculated from the contact angles of the front side irradiated in air (more details on the calculation of the coverage will be discussed in 4.3.2).
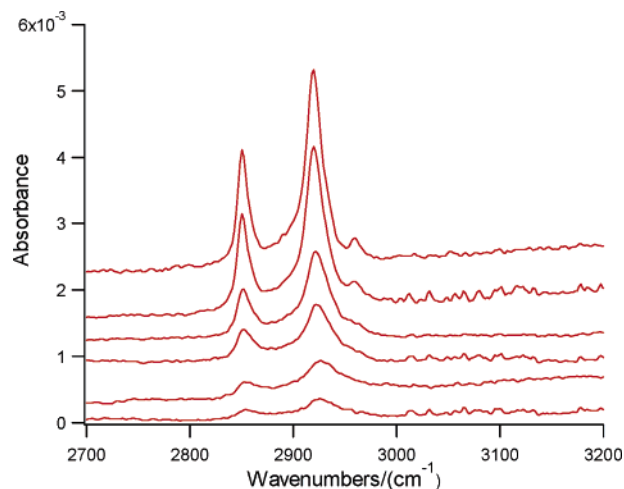

Figure 3. FT-IR spectra of ODS SAMs on glass irradiated for different amounts of time, 0, 5, 20, 30, 45, 60 min in descending order. Spectra are offset for clarity.

carboxylic acids, or increasing coverage of the hydrophilic substrate due to loss of the alkyl chains during the UV irradiation. When the UV irradiation chamber was flushed with argon, there was little change in the contact angle after irradiation. This suggests that the UV alone cannot directly dissociate the alkyl chains at a significant rate. Remarkably, the side of the slides facing away from the irradiation source displayed very low reactivity. The lifetime of ozone is sufficient to maintain a roughly uniform concentration across the UV chamber.[41] As the glass slides are opaque to UV wavelengths below 300 nm, the backside of the sample is exposed to ozone but not UV with wavelength below 300 nm. This result suggests that UV and O_2 are both necessary for the reaction to proceed. In agreement with Moon et al.,[34] we conclude that ozone alone was not the active reagent in our system.

3.2. FT-IR Results.

3.2.1. Degradation Kinetics. The FT-IR spectra in the CH stretch region of the ODS SAMs as a function of irradiation time on glass are shown in Figure 3. $\nu_{as}CH_3$ (CH_3 asymmetric stretch mode near 2960 cm^{-1}), $\nu_{as}CH_2$ (CH_2 antisymmetric stretch mode near 2920 cm^{-1}), and ν_sCH_2 (CH_2 symmetric stretch near 2850 cm^{-1}) modes were resolved. The spectra were
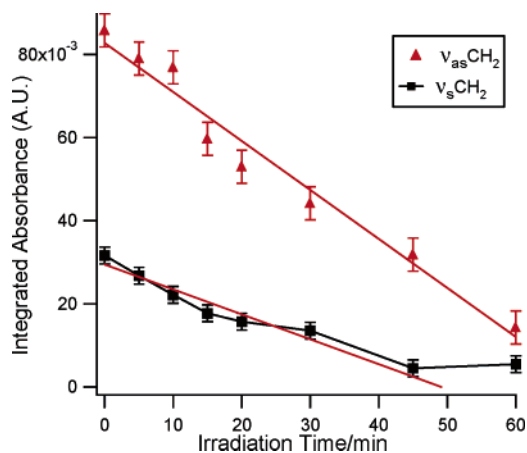
Figure 4. Integrated absorbance of $\nu_{as}CH_2$ and ν_sCH_2 vs UV irradiation time (min).

in good agreement with those reported for compact monolayers in the literature.[42,43] To perform a more quantitative analysis, we deconvoluted the spectra to calculate the integrated absorbance of $\nu_{as}CH_2$ and ν_sCH_2. 80% reduction of the $\nu_{as}CH_2$ and ν_sCH_2 band is observed in Figure 4 after 1 h of UV irradiation in air. The reduction in absorbance suggests conversion of CH_2 groups to other functional groups as well as loss of carbon from the surface. In sharp contrast to the reaction between organic thin films and atomic oxygen under vacuum,[44] which displayed first-order kinetics, the decay rates of the ν_sCH_2 and the ν_{as}-CH_2 mode absorbances did not decrease significantly as the UV degradation proceeded. Instead, the reaction displays roughly zeroth-order kinetics until most of the hydrocarbon groups are depleted, indicating that the reaction rate does not depend on the concentration of CH_2 groups. This result also stands in contrast with previous studies of ambient UV degradation alkanethiol monolayers, which display a decrease in the CH_2 decay rate as the oxidation proceeds.[33] Further analysis of the degradation kinetics can be found in the discussion section.

3.2.2. Compactness of Irradiated SAMs. The peak frequencies and widths of the CH stretch modes are sensitive to the local chemical environment.[43] The CH_2 peak frequency is considered to be a measure of degree of ordering in SAMs.[43] The $\nu_{as}CH_2$ peak frequency is at 2927 cm^{-1} for liquid OTS and 2917 cm^{-1} for solid OTS.[43] At full monolayer coverage, the monolayer has to adopt an ordered configuration to accommodate the maximum number of molecules. The peak frequency of the SAMs we used in this particular experiment is 2920 cm^{-1}, indicating that the film is largely compact but contains a slight amount of disordering. After 45 min of reaction the peak frequency was at 2926 cm^{-1}, close to that in the liquid phase. Our results suggest that the SAM became more disordered as the degradation proceeded as indicated by the blue shift of the CH stretch modes (Figure 5).

3.2.3. Effect of Rinsing. Rinsing the irradiated SAMs in solvents does not change the FT-IR spectra significantly (Figure 6). The robustness of SAMs against rinsing indicates that all remaining CH chains in irradiated SAMs are firmly attached to the surface. It also suggests that the photocleaved species are volatile and therefore removed during the irradiation (prior to rinsing). In contrast, dramatic differences in the CH stretch mode intensity are often observed on irradiated alkanethiol SAM samples before and after rinsing.[3] In the photooxidation of alkanethiol SAMs, the thiolate headgroups react to weaken the bonds to the substrate, forming weakly bonded long alkyl chains that do not evaporate easily and can only be rinsed off with
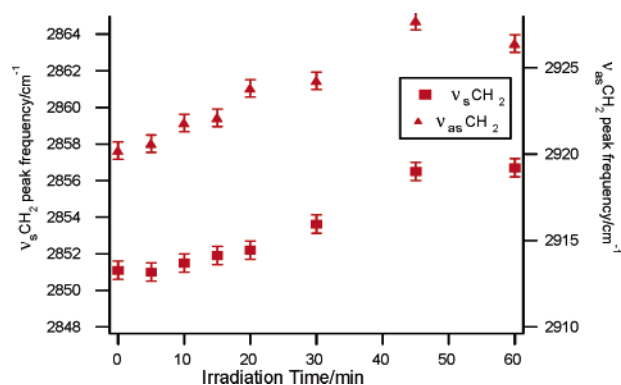

Figure 5. $\nu_{as}CH_2$ and ν_sCH_2 peak frequencies of ODS SAMs as a function of UV irradiation time.
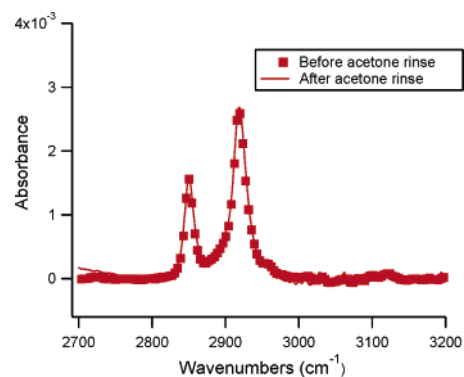

Figure 6. Effect of acetone rinsing on a SAM exposed to 15 min of UV irradiation. The square trace represents the FTIR spectrum acquired immediately after UV irradiation and the solid line is the spectrum of the same sample that was sonicated in acetone for 5 min and dried in ambient.
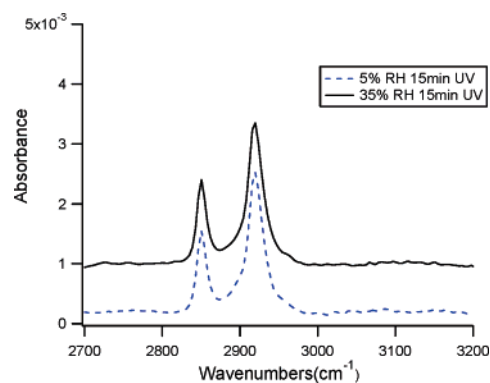

Figure 7. FT-IR spectra of ODS monolayers on glass irradiated with UV for 15 min under 35 and 5% relative humidity.

solvent. This suggests a lack of reactivity in the siloxane headgroups of the ODS monolayers.

3.2.4. Effect of Humidity. To understand the role of water in the system, the UV ozone chamber was placed in a glovebag continuously purged with dry air to reduce the humidity to 5%. Remarkably, the FT-IR spectrum was similar to the spectrum of monolayer irradiated under 35% ambient humidity (Figure 7). The integrated absorbance in the CH_2 asymmetric mode was 0.065 in both cases. This suggests that the changes in concentrations of water vapor, and presumably OH radicals, do not alter the reaction kinetics.

3.2.5. Detection of Other Functional Groups. While our initial experiments focused on the CH stretch region (2800–3000 cm^{-1}), FT-IR should be capable, in principle, of detecting the resulting hydrophilic functional groups formed on the SAM

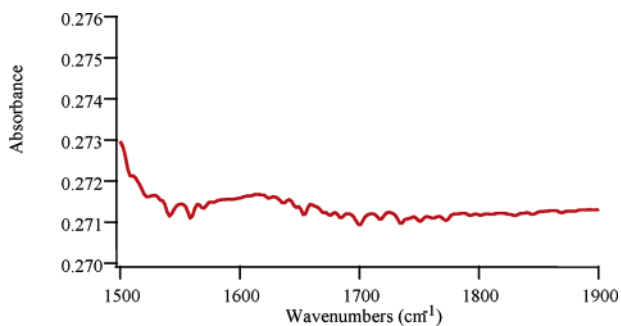Photoreactivity of Alkylsiloxane Monolayers

J. Phys. Chem. B, Vol. 109, No. 20, 2005 **9931**

Figure 8. FTIR spectrum of ODS SAM irradiated for 30 min in the carbonyl stretch region. Substrate SiO$_2$/Si.

Figure 9. XPS spectra of ODS SAMs with no irradiation and after 15 min of UV irradiation. Substrate: SiO$_2$/Si.

surface as well. Carbonyls such as ketones, aldehydes, and carboxylic acids have absorbance near 1700 cm^{-1}. However, the FTIR spectra were inconclusive as to their presence. No peaks can be clearly assigned to carbonyls (Figure 8). Difficulties associated with the detection of carbonyl groups include:

(1) A gas-phase IR water adsorption band near 1700 cm^{-1} overlaps with the carbonyl stretch modes. It is difficult to completely subtract out the background due to the presence of water vapor even with good purging in FT-IR spectrometers.[45]

(2) The signal level from submonolayer species is very small. Assume that the minimum detectable carbonyl signal in an IR experiment is 0.1 mOD. A typical IR cross-section for a C=O group is 8.4×10^{-19} cm^2, calculated from IR data for acetone.[46] Using these two pieces of information, we can calculate that there would have to be 2.7×10^{14} cm^{-2} carbonyl groups at the surface to achieve 0.1 mOD magnitude of signal. A full compact OTS monolayer corresponds to approximately 4.2×10^{14} molecules cm^{-2}. The surface coverage of carbonyls must be greater than 0.65 monolayer to achieve a detectable signal level by FT-IR. This suggests that the surface concentration of carbonyls is less than monolayer coverage and other more sensitive tools are necessary to detect the surface functionalities.

3.3. XPS Results. To determine the chemical composition of irradiated SAMs, XPS spectra were collected on ODS SAMs with and without UV irradiation. After 15 min of irradiation, the C(1s) intensity was reduced by 12 ± 4%. FT-IR suggests that 31 ± 6% of CH$_2$ groups were lost after 15 min of irradiation. It should be noted that due to the attenuation in photoelectrons, the photoelectron intensity is a sublinear function of the carbon content, i.e., the percentage reduction in the surface concentration of carbon should be higher than 12%. The photoelectrons from thicker the films experience greater attenuation.[47] The attenuation of photoelectrons from atoms covered by a film with a thickness x can be described by the following equation.[47]

$$i = i_0 e^{-x/\lambda \sin \theta} \qquad (1)$$

where i is the intensity after attenuation per unit depth, i_0 corresponds to the unattenuated intensity, λ is the attenuation length of photoelectrons, and θ is the take off angle with respect to the surface.

For a uniform organic film consisting of n alkyl chains with thickness d, the total photoelectron intensity, I, if the film can be obtained by integrating the intensity at different depths x (distance from the vacuum air interface).[47]

$$I = \int_0^d i_0 e^{-x/\lambda \sin \theta} dx = i_0 \lambda \sin \theta (1 - e^{-d/\lambda \sin \theta}) =$$
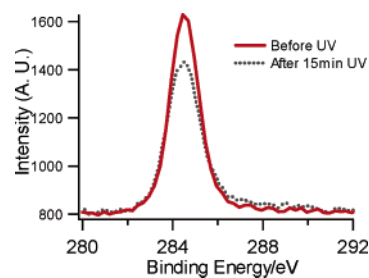$$I_\infty (1 - e^{-d/\lambda \sin \theta}) \quad (2)$$

where I_∞ corresponds to the total intensity from an organic film with infinite thickness.

We assumed the thickness of the hydrocarbon layer of the unirradiated ODS SAM to be 25 Å and the λ of C(1s) photoelectron to be 32 Å[47] and θ is 60°. According to eq 2, a decrease of total intensity of 12 ± 4% after UV irradiation corresponds to a reduction of the layer thickness by 18 ± 5%. It should be mentioned that there is significant uncertainty in the value of the λ of C(1s) photoelectrons in hydrocarbon films.[47,48] Therefore, we are unable to conclude whether the difference of loss of carbon measured by XPS and the loss of methylene groups measured by FT-IR is significant.

In addition, part of the difference between XPS and FTIR results may be accounted for by the appearance of several % coverage of various oxygen containing groups (CO$_2$H, COH, and CO) as discussed below. There were some indications of shoulder peaks at C−O (286.5 eV) and C=O (290 eV). However, the peaks were too low for quantitative measurement. The upper limit of oxygenated carbon is estimated to be 8% by integrating the fitting residue of a Voigt function centered at 285 eV. In addition, as the SAM degrades, it may be less resistant to contamination. Therefore, we cannot exclude the possibility that the adsorption of hydrocarbon contamination from the ambient during the time window after UV irradiation and before loading the sample to the XPS chamber. Overall, our results suggest that the oxygenated content is small. (As will be presented in the next section, we used fluorescence labeling to identify functional groups chemically attached to SAMs. Physisorbed functional groups do not contribute to the fluorescence signal in this case.)

We note that other XPS studies of UV photooxidation of ODS SAMs did not find an appreciable amount of oxygenated carbon with XPS.[8,34] In contrast, Paz. et al. found a pronounced shoulder peak in the C(1s) region after treating ODS SAMs with O(^{3}P), suggesting that more than 20% of the carbon is converted to oxygen when a similar total amount of carbon is lost.[44] Similarly, the shoulder peaks for oxygenated carbon of ODS SAMs were significantly more pronounced under the X-ray or electron beam irradiation in a vacuum or low-pressure oxygen.[5,27] It suggests that once formed, the oxygenated functional groups are more readily cleaved under the UV/oxygen environment. By comparison, due to the lack of ambient oxidants, the oxygenated functional groups may accumulate on the surface under low oxygen environments, such as in a vacuum chamber.[44]

3.4. Fluorescence Labeling of Surface Species (FLOSS). Although we suspected the presence of oxygen containing functionality in UV-irradiated siloxane SAMs, these could not be detected with FTIR or XPS. UV/O$_3$ irradiation may produce surface densities of the OH, CHO, and COOH functional groups in the range of 0.01 ML (ML is defined as the maximum surface concentration of packed alkyl chains, 4.2×10^{14} cm^{-2}).[49] Recently, we developed FLOSS to detect low concentration
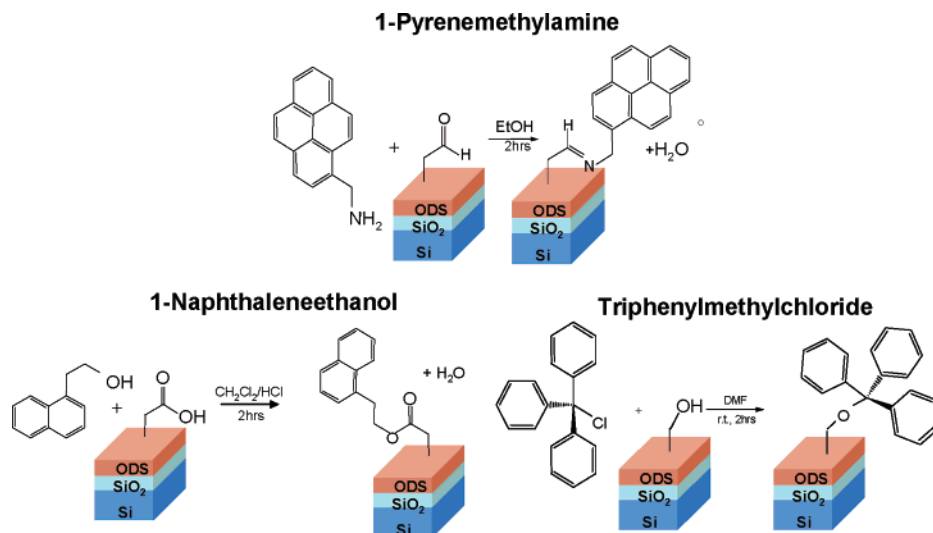
Figure 10. Schematic of fluorescence labeling of CHO, COOH, and OH surface functional groups.
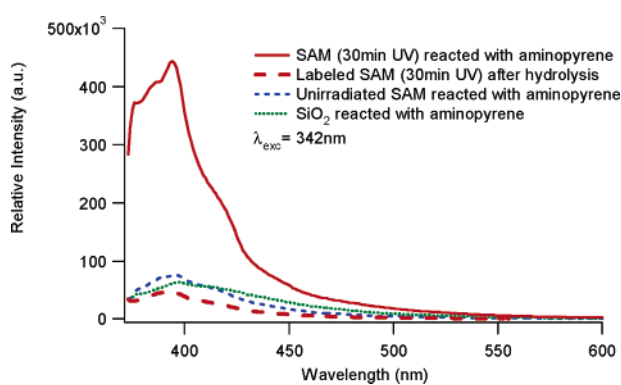

Figure 11. Detection of surface aldehyde/ketone groups by covalent surface attachment of 1-pyrenemethylamine to a SAM surface irradiated for 30 min in UV/O$_3$ and controls. The emission from the labeled SAM dropped dramatically after 1 h of hydrolysis.
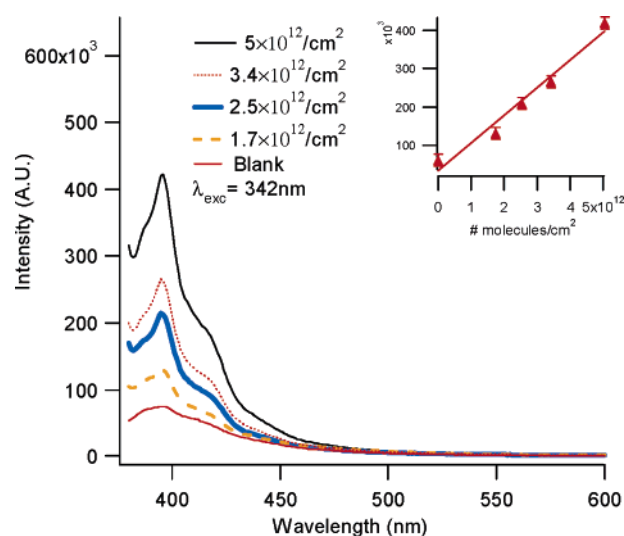

Figure 12. Emission spectra of different amounts of aminopyrene deposited on ODS SAM surface and the calibration plot (inset). (The calibration plot reported in Figure 2 of ref 50 is in error by a factor of 1/0.24, corresponding to the fluorescing area of the sample. Data for aldehyde concentrations in Figure 4 of ref 50 were derived from a correct version of Figure 2.)

surface functionalities.[50] In the area of biological[51–55] and polymer chemistry,[56–59] fluorescent labeling has long been used to both qualitatively and quantitatively monitor functionality. Fluorescent probes have also been used study the structure and reactivity of SAMs.[36,60–62]

1-Pyrenemethylamine was selected to label aldehyde and/or ketone surface groups by formation of imine linkages, as shown in Figure 10. (Formation of amide by a reaction between carboxylic acid and amine groups cannot occur at room temperature.[63]) Naphthaleneethanol was used to label carboxylic acid surface groups by formation of esters. Triphenylmethlyl chloride was selected to identify surface OH groups.

As an example, the presence of CHO on UV-irradiated SAMs was indicated by the covalent attachment of 1-pyrenemethyl-amine. The fluorescence from irradiated monolayers, which presumably contained oxygen functionality, was significantly more intense than from the unirradiated monolayer or bare substrate, which underwent the same labeling reaction (Figure 11). This suggests that nonspecific adsorption is relatively weak, and that the majority of the chromophores can be rinsed off the unirradiated SAM or bare substrate. By contrast, when surface carbonyl groups are present, chromophores are covalently attached and can survive prolonged rinsing. To further prove that the chromophores are attached to the surface via imine linkage, the labeled SAM was subjected to hydrolysis for 1 h by a catalytic amount of H$_2$SO$_4$, which could presumably cleave the imine bond (Figure 11). Indeed, after hydrolysis the emission was reduced to the background level.

Reinhoudt et al. found that the fluorescence from ~0.3 ML pyrene attached to a NH$_2$ terminated SAM is dominated by excimer emission around 480 nm.[62] In contrast, as shown in Figure 11, the emission in UV-irradiated SAMs is dominated by monomer emission near 390 nm. This provides evidence that the surface coverage of the attached pyrene was probably less than 0.1 ML, and that there was no significant clustering of surface aldehyde/ketone groups. Due to the large distances between the covalently attached chromophores, little aggregation could occur.

To quantify the amount of chemisorbed chromophores, corresponding to different chemical functionalities in irradiated SAMs, calibration curves were obtained by measuring the peak fluorescence intensities for known amounts of chromophores deposited on an unirradiated SAM surface. Deposition of chromophores was achieved by uniformly spreading a predetermined volume of chromophore solution on the surface and letting the solvent evaporate (Figure 12). At small surface concentrations, the emission increases nearly linearly as a function of the amount of deposited chromophores. By measuring the peak intensity of the surface labeled by the corresponding

Photoreactivity of Alkylsiloxane Monolayers

J. Phys. Chem. B, Vol. 109, No. 20, 2005 **9933**

chromophores, the surface concentrations of the corresponding functionalities are determined from the calibration plots, such as the inset in Figure 12. From the calibration plot, the fluorescence intensity of the pyrene labeled SAM that had been irradiated for 30 min corresponds to 1.3% of ML of aldehyde/ketone groups. This low coverage is consistent with the afore mentioned conclusion (Figure 11) that little chromophore aggregation occurred. Similarly, other groups such as COOH and OH were detected by FLOSS,[50] and their concentrations appeared to be below a few percent of a monolayer.

It should be noted that FLOSS preferentially detects the functional groups on the top of SAMs. Functional groups buried in the monolayer may not be accessible to chromophores. In addition, the chromophores used are large enough to occupy 3−4 surface sites of close packed alkyl chains. FLOSS is probably not suitable for measuring high concentration surface species (>0.1 ML). If the surface functional groups are closely packed, the chromophores may not be able to attach to all the closely packed surface groups.[62] In addition, chromophore aggregation and fluorescence quenching at high concentrations might make quantification complicated.[62] Therefore, the concentration of functional groups may be underestimated. Future studies, labeling the SAM surfaces with chromophores of different geometries, can address the issue of steric hindrance. On the other hand, this steric limitation can potentially be an advantage of FLOSS, since one may use chromophores with different geometries to access information about lateral and vertical spatial distributions of functional groups (e.g., phase segregation[45]), which is difficult to achieve with XPS or SIMS.

4. Discussion

4.1. Summary of Results.

(1) UV degradation of ODS SAMs requires the combination of UV and oxygen. Ozone alone does not degrade alkylsiloxane SAMs.

(2) Contact angle results suggest that the SAMs become increasingly more hydrophilic. However, water does not completely wet the surface even after several monolayers of CH_2 groups are removed. This suggests the coexistence of hydrophilic and hydrophobic groups on the top of irradiated SAMs.

(3) FT-IR results show a decrease in the number of CH groups. The kinetics is complicated. It is more consistent with zeroth order kinetics than first-order kinetics. The less compact monolayer showed a blue shift (gauche defects) as degradation proceeds.

(4) XPS results showed a loss of carbon. However, the concentration of oxygenated carbon is too low to unambiguously identify.

(5) FLOSS enables the identification and quantification of a small amount of functional groups formed during the UV irradiation. We estimate that the total surface coverage of oxygen containing functional groups (OH, COOH, and CHO) is at most a fraction (<5%) of a monolayer.

4.2. Active Agents.

Our results clearly showed that the UV from our low-pressure Hg lamp alone does not degrade ODS SAMs. Photolysis of saturated SAMs requires a $\sigma - \sigma^*$ transition induced by absorption of photons with wavelengths shorter than 160 nm.[24] Since our UV source (mainly 254 nm and some 183 nm) falls short of the required range, the UV light cannot dissociate the saturated hydrocarbon chains directly. This explains the lack of reactivity when the UV chamber is purged with inert gas. The requirement of the combination of UV and oxygen suggests the role of UV-generated reactive species, such as OH or O, which are known to react with organic monolayers.[18,20,21,44]

TABLE 1: Reactions to Generate Atmospheric Oxidants[40]

$O_2 + h\nu$ (185 nm) $\rightarrow$ 2 O(^{1}D)		R1
$O_3 + h\nu$ (254 nm) $\rightarrow O_2$ + O(^{1}D)	k_1	R2
O(^{1}D) + M $\rightarrow$ O(^{3}P) + M	$k_2 = 5 \times 10^{-11}$ cm^3 molecule^{-1} s^{-1}	R3
O(^{1}D) + $H_2O \rightarrow$ 2HO$^\bullet$	$k_3 = 2.2 \times 10^{-10}$ cm^3 molecule^{-1} s^{-1}	R4
O(^{3}P) + O_2 + M $\rightarrow O_3$ + M	$k_4 = 2 \times 10^{-33}$ cm^6 molecule^{-2} s^{-1}	R5

The photochemistry of O_3, O, and OH are well-known.[30] Under UV irradiation in ambient, ozone is produced in reactions illustrated in reaction schemes R1 and R5 (Table 1). Singlet atomic oxygen O(^{1}D) is produced by photolysis of ozone. OH is mainly produced by the reaction between O(^{1}D) and H_2O (R4). Most of the O(^{1}D) is rapidly quenched by collision with inert molecules (M) such as N_2 (R3).[64] In the ambient environment, the concentration of N_2, 1.9×10^{19} molecule/cm^3, reduces the lifetime of O(^{1}D) to ~1 ns (R3). Only a small fraction (~1%) of O(^{1}D) is able to form OH under ambient (R4). The production rate of OH is proportional to the humidity. The insensitivity of ODS degradation kinetics to humidity (from 5 to 35%) is surprising because OH is widely recognized as the major oxidant of hydrocarbons in the atmosphere.[23] It may suggest that under our conditions, due to higher concentrations or rate constants, other reactive species such as atomic oxygen play dominant roles in hydrogen abstraction and the contribution from OH is negligible. Further investigations, such as measurements of the OH concentration, are necessary to clarify the role of OH radicals. From the preceding discussion, atomic oxygen is a plausible oxidant in ambient UV oxidation of ODS SAMs.

More insights on the role of atomic oxygen can be gained if the concentration of atomic oxygen can be estimated. The production rate of atomic oxygen is shown in eq 3, where I_0 is the UV light intensity, σ is the absorption cross section 1150 $\times 10^{-20}$ cm^2, [40] and $h\nu$ is the photon energy at 254 nm. k_1 is calculated to be 3.2×10^{-2} s^{-1}.

$$\frac{d[O_3]}{dt} = \frac{I_0\sigma}{h\nu}[O_3] = k_1[O_3] \qquad (3)$$

R2 and R5 dominate the equilibrium between ozone and O(^{3}P).[30] Under a steady-state condition,

$$k_1[O_3] = k_4[O_2][M][O(^3P)] \qquad (4)$$

$$[O(^3P)]/[O_3] = \frac{k_1}{k_4[O_2][M]} = 1.3 \times 10^{-7} \qquad (5)$$

The ozone concentration in the UV chamber is 100 ppm (2.4×10^{15} molecule/cm^3), [O(^{3}P)] is estimated to be 3.2×10^8 molecule/cm^3.

The flux[65] of O(^{3}P) is

$$f_{o(3P)} = [O(^3P)] \times \left(\frac{k_B T}{2\pi m}\right)^{1/2} \qquad (6)$$

where k_B is the Boltzmann constant and T is the temperature (300 K) and m is the mass of atomic oxygen. The flux of O(^{3}P) is calculated to be 5.2×10^{12} molecule cm^{-2} s^{-1}. Similarly, the flux of O(^{1}D) is calculated to be 9.8×10^8 molecule cm^{-2} s^{-1}. Assuming the area of a hydrocarbon chain to be 0.225 nm^2,[43] the total surface concentration of hydrocarbon groups (CH_2 and CH_3) in a compact ODS SAM is equivalent to 7.6×10^{15} groups cm^{-2}. The time to completely oxidize the ODS SAM is observed to be about 4200 s. Therefore, the average

reaction rate R_{CH} is 1.8×10^{12} molecule cm^{-2} s^{-1}. The flux of O(^{1}D) is too low to account for the oxidation of ODS. However, the flux of O(^{3}P), 5.2×10^{12} molecule cm^{-2} s^{-1} compares favorably to R_{CH}, considering the high reaction probability of hydrogen abstraction by O or OH on organic surfaces.[18,44]

4.3. Reactive Sites.

4.3.1. Headgroups vs Alkyl Chains. In our previous report, the AFM results suggested that the defect sites in ODS SAMs are not important in the degradation and that the chains of the ODS molecules are gradually shortened.[30] The FT-IR spectrum of a UV-irradiated SAM after acetone rinsing in Figure 6 revealed no significant difference in CH stretch, further supporting that the degradation products are volatile small molecular weight compounds and no significant amount of long alkyl chains, products of scission at the headgroups, are generated. This stands in contrast to the degradation mode of alkanethiol SAMs, where the degradation initiates preferentially at the defect sites and oxidation of headgroups produce large amount of solvent-labile species that remain on the surface.[3] All these results suggest that the headgroups in alkylsiloxane SAMs have negligible reactivity. The difference can be explained by the different chemical reactivity of the two systems. The terminal thiolate group, with its lone pairs, can be oxidized without cleavage of other bonds. In fact, gas-phase oxidation of thiols with atomic oxygen showed nearly zero reaction activation barrier.[66] By contrast, to oxidize the valence saturated siloxane group, cleavage of the Si−C bond (bond energy ≈ 300 kJ/mol[67]) is required. This renders the oxidation of the siloxane headgroup kinetically unfavorable.

4.3.2. Preferential Reactive Sites in the CH Chains. Having settled that the degradation of ODS proceeds via the photooxidation of alkyl chains instead of headgroups and that the process is initiated by a series hydrogen abstraction reactions, we can focus on the molecular scale mechanism of alkyl chain oxidation. The pseudo zeroth-order CH$_2$ decay kinetics that we observe under ambient (Figure 4) contrasts with the first-order reaction between O(^{3}P) and alkyl organic thin films under vacuum.[44] Paz et al. found that the reaction between O(^{3}P) and hydrocarbon chains in SAMs under a vacuum environment is limited by the penetration of O(^{3}P).[44] The oxygenated functional groups may accumulate on the surface under vacuum, where oxidative species are present at lower concentrations, blocking the access of reactive species to the underlying hydrocarbon groups.[44] We propose that under an ambient environment, the high concentrations of dioxygen or ozone results in much more efficient cleavage of oxygenated functional groups.

A straightforward interpretation of the kinetics is the constant effective surface concentration of CH$_2$ on the surface as degradation proceeds. This requires that the monolayer degradation preferentially initiate from the top of a SAM, which is more accessible to reactive species. The loss of CH$_2$ signal is mainly due to the loss of carbon, exposing the underlying groups for hydrogen abstraction. Under an ambient environment, where the terminal group of a chain is cleaved, the effective surface concentration of CH$_2$ remains the same as long as all the 17 carbon groups in a chain are not cleaved.

$$R = \frac{d[CH_2]}{dt} = k[CH_2] \qquad (7)$$

$$[CH_2] \equiv ML \qquad (8)$$

From this pseudo-zeroth order kinetics (eqs 7 and 8), we can extract the nominal reaction rate constant of CH$_2$ groups by assuming the effective surface concentration to be a monolayer. From the slope in Figure 4, k_{CH_2} is calculated to be 4.1×10^{-3} s^{-1}, under our conditions.

More detailed analysis of contact angle results affords additional information about the microscopic mechanism. The contact angle measurements indicate that the hydrophobic CH$_3$ and CH$_2$ groups (contact angle ∼ 110°) are converted to hydrophilic groups such as CHO, OH, and COOH (contact angle ∼ 0° [68]) during degradation (Figure 2). However, even after 30 min of degradation, when half of the CH$_2$ groups are lost, according to FTIR (Figure 4), the contact angle still has not dropped to zero. This suggests that the surface is still not completely covered with hydrophilic groups. The contact angle of a composite surface mixed on a molecular level is described by[68]

$$(1 + \cos \theta)^2 = f_1(1 + \cos \theta_1)^2 + f_2(1 + \cos \theta_2)^2 \qquad (9)$$

where θ, θ_1, and θ_2 are the contact angles on the composite surface, hydrophilic surface, and hydrophobic surface, respectively. f_1 is the fractional coverage of the hydrophilic groups, and f_2 is the fractional coverage of the hydrophobic groups. Assuming θ_1 to be 0 and θ_2 to be 110 degrees, the fractional coverage of the hydrophilic groups can be calculated from the measured contact angle θ (Figure 2). It is to be noted that the fractional coverage does not necessarily correspond to the physical surface composition because it does not take into account the effect of surface reconstruction during wetting, as well as the degree of probe molecular penetration.[68] Nevertheless, this approach provides qualitative insights into the relative contribution of different surface groups to the overall wetting. According to FT-IR results in Figure 4, 25% of CH$_2$ groups are lost after 15 min of UV irradiation, corresponding to more than four monolayers of CH$_2$ groups since each ODS molecule contains 17 CH$_2$ units. Yet, the effective fractional coverage of hydrophilic groups indicated by contact angle is only about 30% (Figure 2) when more than 4 ML of CH$_2$ groups are lost. This suggests that only a fraction of the top of the reacted monolayer is covered with hydrophilic groups.

There are several possible explanations for the more gradual increase of the effective coverage of hydrophilic groups.

(1) The oxygenated groups are buried in the monolayer and are therefore not accessible to water molecules used in contact angle measurements, contributing less to the effective surface coverage of the hydrophilic groups.

(2) Even if all the top of the monolayer is completely converted to hydrophilic groups, the top of the SAM surface may be rough and the water used to measure the contact angle is in contact with the hydrophilic top as well as the hydrophobic side chains (Figure 13C).

(3) The reaction of the CH groups does not necessarily lead to conversion to hydrophilic groups. Some of the radicals may recombine, leading to cross-linking (Figure 13D2).

With the information we have about the nature of the reactant and reactive sites in the ODS SAMs, four possible mechanisms are listed (Figure 13).

Mechanism A: Chain scission occurs at the Si−C bond and reaction nucleates from the defect sites.

Mechanism B: Hydrocarbon chain scission occurs exclusively at the top of the monolayer and the degree of chain scission is uniform. Consequently, the top of the monolayer is uniformly terminated with hydrophilic groups.
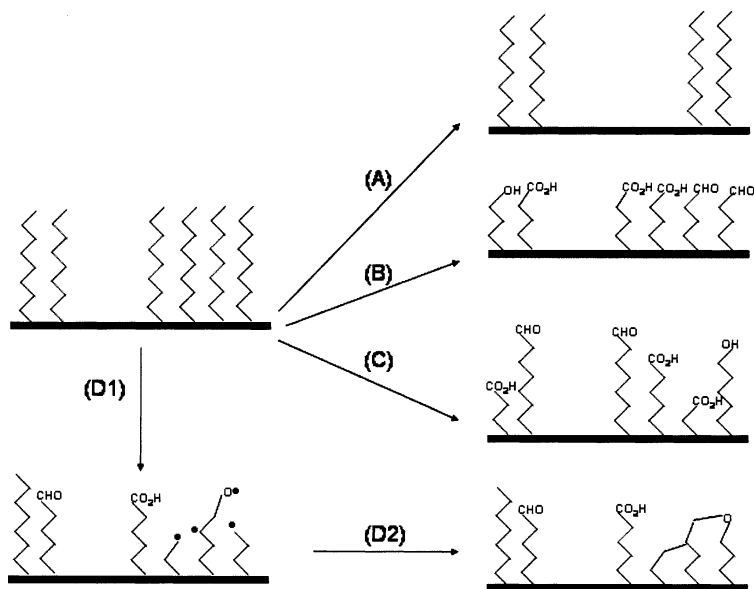
Photoreactivity of Alkylsiloxane Monolayers

J. Phys. Chem. B, Vol. 109, No. 20, 2005 **9935**

Figure 13. Possible microscopic mechanisms of alkylsiloxane degradation.

Mechanism C: The reaction is restricted to the top of the hydrocarbon chains; loss of carbon occurs randomly.

Mechanism D: The chain scission is not limited to the top of the CH chains. Atomic oxygen and other reactive species may penetrate a few groups deep into the monolayer and react with the side of the CH chains. Radicals resulting from hydrogen abstraction may recombine (cross-link).

Mechanism A can be easily excluded as discussed above. Mechanism B is not consistent with the observation that the contact angle does not drop to zero even after several monolayers of CH_2 is removed. If the top of the SAM were uniformly terminated with hydrophilic groups, the contact angle should be close to zero within 10 min.[69]

To better understand the resultant nanometer scale morphology of mechanism C, we carried out a computer simulation assuming the following:

(1) Only the top of a CH chain can react.

(2) The reaction results in the loss of one CH group (CH_2 or CH_3) each time.

(3) The reaction on the top of CH chains occurs with equal probability (totally random) regardless of the local environment.

The evolution of the simulated morphology is shown in Figure 14. It is apparent that such random chain scission introduced significantly roughness, i.e., different chains lose different numbers of CH groups.

The average fractional coverages of the different hydrocarbons groups and the RMS roughness are shown in Figure 15. The decay rate of the CH_2 group is mostly constant except in the initial and final stages. The zeroth order kinetics is due to the constant effective surface concentration of CH_2 groups. When a CH_2 group is cleaved, the underlying CH_2 group is exposed. Therefore, the effective surface concentration remains the same. The initial slower rate is attributed to the presence of CH_3 groups, blocking the access of reactive species to the underlying CH_2 groups. The decreased rate at the later stage is due to the depletion of CH_2 groups. Once all the CH_2 groups in a surface site are reacted, this site can no longer participate in the chain scission reaction. Hence, the effective surface concentration of CH_2 groups decreases. The reaction kinetics from the simulation is consistent with the IR results in Figure 4 in reproducing the roughly constant decay rate of CH_2 stretch modes. However, due to the limited precision of the measured

absorbance, it is difficult to conclude from the IR data whether the reaction rate is slower at the initial and the late stages the irradiation, as suggested by mechanism C.

The RMS roughness can be as much as the height of five CH_2 groups (Figure 15). Although the nonuniform chain scission introduces microscopic scale roughness, the roughness is on the nanometer scale and consequently cannot be observed with the limited lateral resolution of AFM (10 nm).[30] However, such microscopic scale roughness is consistent with the fact that the water contact angle does not drop to zero after 20 min (Figure 2), when several monolayers of CH_2 groups are removed. During the contact angle measurement, water is in contact with morphologically and chemically heterogeneous surfaces. The hydrophilic top, as well as the hydrophobic side, of chains of the UV-irradiated SAMs are exposed to water during contact angle measurements. This roughness may also explain the blue shift in the CH stretch region in the IR spectrum of irradiation SAMs (Figure 5). Due to the roughness on the surface, the top portion of CH chains has more free space, similar to a liquid environment.

However, this mechanism does not explain the observation that the hydrophilic groups cover only a fraction of monolayer, as suggested by FLOSS. It may be caused by the microscopic roughness of SAMs as the bulky chromophores cannot label the functional groups at the bottom of the pinholes produced by UV irradiation. Or it may indeed suggest only a small fraction of the monolayer is functionalized by those oxygenated functional groups. This raises the possibility of mechanism D.

It is also possible that the reactive species penetrate a few groups deep into the ODS SAM as suggested by mechanism D (Figure 13). In addition, the radicals formed during hydrogen abstraction process may recombine, leading to cross-linking. Cross-linking is believed to be prevalent in electron beam or X-ray induced degradation of SAMs.[26,28] Mechanism D generates a surface with even lower coverage of hydrophilic groups due to the presence of cross-linking. Therefore, not all chain scission events result in the formation of hydrophilic groups. This appears to be consistent with the FLOSS results that only a fraction of a monolayer is functionalized.

4.4. Probable Reaction Pathways. The hydrocarbon chains are gradually shortened during photooxidation. FT-IR results point to a microscopic reaction pathway that involves the
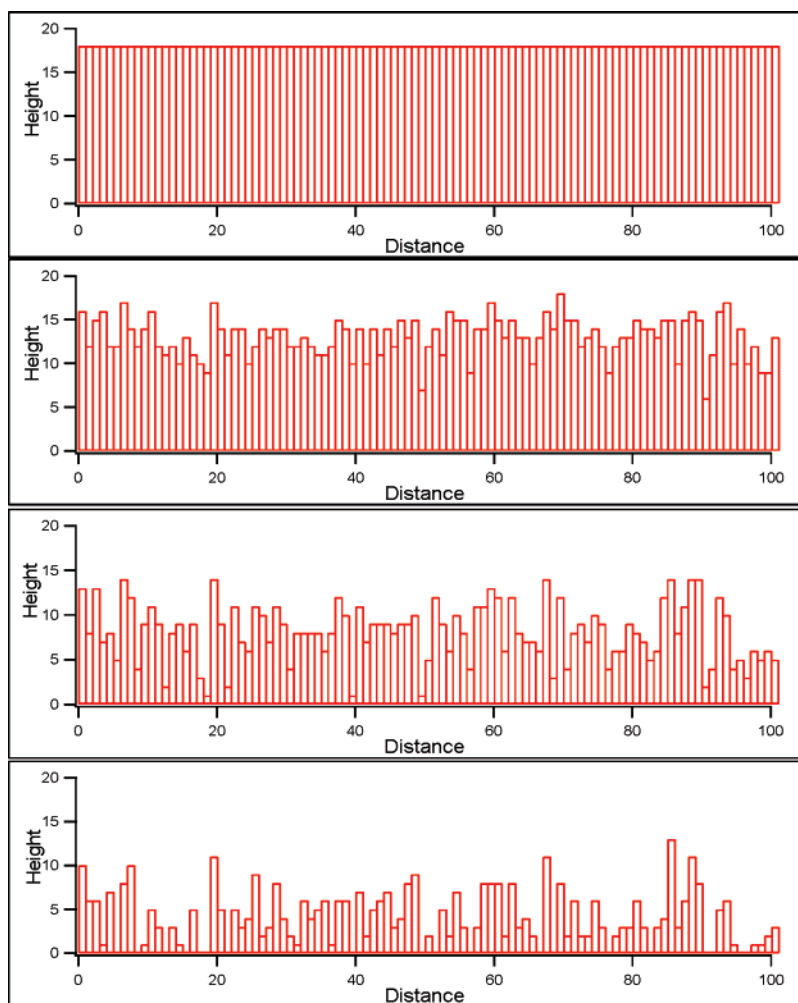
Figure 14. Simulated evolution (top to bottom) of a morphological cross section of ODS SAM. Each bar represents an individual ODS chain. Height is in the unit of the height of a CH$_2$ group (~0.14 nm). Horizontal distance is in units of the lateral spacing between chains (~0.5 nm).
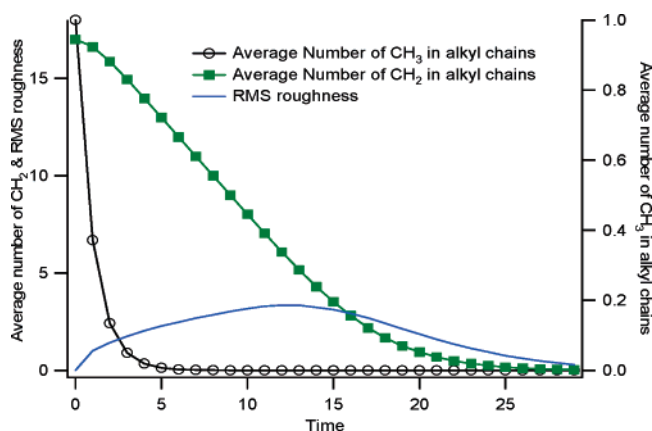

Figure 15. Evolution of simulated morphology assuming that chain scission is restricted to the top of chains. Each time increment represents the time it takes to react 1 ML of surface sites.

reactivity of hydrocarbon chains instead of siloxane headgroups. We assume that the mechanism of UV degradation of alkyl chains in SAMs also involves hydrogen abstraction as it does in the gas phase.[70] It is to be noted that even in the gas phase, photooxidation of compounds as simple as butane can have extremely complex reaction pathways.[19] It is much more difficult to access information about the individual steps in the condensed phase such as SAMs.

However, given the evidence of the role of atomic oxygen in the UV degradation of ODS SAMs and the detection of

TABLE 2: Formation of Alkoxy Radical

$R-H + O \rightarrow R^{\bullet} + HO^{\bullet}$	R6
$R^{\bullet} + O_2 \rightarrow ROO^{\bullet}$	R7
$ROO^{\bullet} + h\nu \rightarrow RO^{\bullet} + O$	R8
$ROO^{\bullet} + HO^{\bullet} \rightarrow RO^{\bullet} + HOO^{\bullet}$	R9

TABLE 3: Further Oxidation

$RCH_2O^{\bullet} + O_2 \rightarrow RCHO + HOO^{\bullet}$	R10
$RCHO + h\nu \rightarrow R^{\bullet} + CHO^{\bullet}$	R11
$RCH_2CHO + O \rightarrow RCH^{\bullet}CHO + HO^{\bullet}$	R12
$RCH^{\bullet}CHO \rightarrow RCH_2^{\bullet} + CO$	R13
$RCHO + O \rightarrow RCO^{\bullet}$	R14
$RCO^{\bullet} + O_2 \rightarrow RC(O) O_2^{\bullet}$	R15

reaction intermediates such as alcohol, carbonyls, and carboxylic acid groups by FLOSS, we can propose a plausible reaction pathway (Tables 2 and 3). The first step probably involves hydrogen abstraction to form alkyl radicals (R6). The alkyl radicals rapidly react with O$_2$ to form peroxide radicals (R7). As illustrated in R8 and R9, the peroxide has a number of pathways to form alkoxy radicals, which can be oxidized to form carbonyls (R10). The aldehyde groups can dissociate via photolysis (R11) or further hydrogen abstraction at the α carbon (R12 and R13), finally resulting in loss of carbon. Hydrogen abstraction in the CHO group (R14) results in the formation of peroxyacids (R15), a precursor of carboxylic acids.

4.5. Implications on Photopatterning. A key requirement for photopatterning is to limit oxidation to the irradiated areas. This requirement can be easily fulfilled if the photons can excite

Photoreactivity of Alkylsiloxane Monolayers

J. Phys. Chem. B, Vol. 109, No. 20, 2005 **9937**

the SAMs directly.[7] However, we observed that chemical reactants, such as O(^{3}P), are necessary for the UV degradation of ODS SAMs when wavelengths of 184 nm or longer are employed. These chemical reactants may not be confined to irradiated areas. From the right side of eq 4, the lifetime of O(^{3}P), the reciprocal of $k_4[O_2][M]$, is calculated to be 4.2 × 10^{-6} s. The diffusion coefficient of O(^{3}P) under 1 atm is D = 1 cm^2 s^{-1}.[18]

The free mean path of O(^{3}P) can be estimated by

$$l = \sqrt{D\tau} = 17 \,\mu m \qquad (10)$$

Therefore, the reactive species O(^{3}P), which is mainly responsible for hydrogen abstraction, can diffuse tens of micrometers away from the irradiated areas, resulting in poor resolution in projection photopatterning of SAMs. Therefore, if the degradation process is dominated by chemical reactions, to achieve good resolution, proximity masks are necessary to reduce the diffusion of reactants to undesired areas.

However, at 5 W/cm^2 intensity, projection UV photopatterning of alkyl-based SAMs has been reported to achieve submicron resolution.[11] Clearly, photolysis is involved in that case. This apparently contradictory observation can be understood in the context of the following. The hydrogen abstraction, the first step of oxidation of aliphatic chains, involves radicals that may not have high spatial confinement. However, photolysis, whose spatial resolution is only limited by the spatial confinement of irradiation, may occur on reaction intermediates. The loss of carbon is probably due to the removal of CHO groups by hydrogen abstraction at the α carbon or the photolysis of CHO. The effective rate constant of photolysis of aldehydes can be estimated from the intensity of the UV light assuming unity quantum yield.

$$\frac{d[CHO]}{dt} = \frac{I_0\sigma}{h\nu}[CHO] = k'[CHO] \qquad (11)$$

where I_0 (2 mW/cm^2) is the incident intensity of UV irradiation, σ is the absorption cross section (2 × 10^{-20} cm^2),[71] and $h\nu$ is the photon energy (7.8 × 10^{-19} J).

We found the rate constant to be 5.1 × 10^{-5} s^{-1}, nearly 2 orders of magnitude lower than k_{CH_2} (4.1 × 10^{-3} s^{-1}). Therefore, photolysis is not the dominant channel for dissociation of carbonyls at this low intensity. Rather, we suggest that the loss of carbon mainly results from the reaction of chemical reactive species, e.g., hydrogen abstraction at the α carbon site (R12). Another important step, that photolysis may significantly contribute to, is the photodissociation of peroxide radicals into alkoxy radicals (R8). The reported cross section is 360 × 10^{-20} cm^2 at 254 nm,[72] which results in a rate constant of 1 × 10^{-2} s^{-1}. However, the contribution from competing chemical reactions such as R9, is unknown. Therefore, it is not clear whether the photolysis channels, such as R8, dominate.

A better understanding of the mechanism of ODS photoreactivity can provide insight into how to favor the reaction pathways that have better spatial confinement during photopatterning processes. One can envision that even if the light photon energy is not in the range of direct photolysis of alkyl chains, by increasing light intensity and other reaction conditions, the contribution from photolysis can be increased relative to the contribution from chemical reactions.

4.6. Conclusions. In conclusion, our combination of different surface characterization techniques has enabled new molecular level insight into the mechanism of the UV photoreactivity of ODS SAMs in terms of reactive agents, reactive sites, kinetics, and reaction pathways. Our results provide evidence that atomic oxygen O(^{3}P) is the primary reactive agent for the UV degradation of ODS SAMs. UV degradation results in the scission of alkyl chains instead of the siloxane headgroups. Our results suggest that the top of the ODS SAMs is the preferential reactive sites. Using a novel, highly surface sensitive technique, FLOSS, we identified the presence of submonolayer quantities chemical functional groups formed by the UV degradation. We proposed a mechanism based on hydrogen abstraction. Our investigation helps to clarify the role of alkyl chains in the photoreactivity of SAMs. Our investigation also has implications in optimizing photopatterning of SAMs. We believe that such molecular level understandings of SAM reactivity will become increasingly important in high-resolution photoresist micropatterning as the resolution may start to be limited by the size of the resist and spatial extent of the photochemical reactions.[22]

References and Notes

(1) Ulman, A. *Chem. Rev.* **1996**, *96*, 1533.
(2) Poirier, G. E.; Herne, T. M.; Miller, C. C.; Tarlov, M. J. *J. Am. Chem. Soc.* **1999**, *121*, 9703.
(3) Zhang, Y. M.; Terrill, R. H.; Tanzer, T. A.; Bohn, P. W. *J. Am. Chem. Soc.* **1998**, *120*, 2654.
(4) Huang, J. Y.; Hemminger, J. C. *J. Am. Chem. Soc.* **1993**, *115*, 3342.
(5) Lercel, M. J.; Whelan, C. S.; Craighead, H. G.; Seshadri, K.; Allara, D. L. *J. Vac. Sci. Technol. B* **1996**, *14*.
(6) Hoeppener, S.; Maoz, R.; Cohen, S. R.; Chi, L. F.; Fuchs, H.; Sagiv, J. *Adv. Mater.* **2002**, *14*, 1036.
(7) Dulcey, C. S.; Georger, J. H., Jr.; Krauthamer, V.; Stenger, D.; Fare, T. L.; Calvert, J. M. *Science* **1991**, *252*, 551.
(8) Sugimura, H.; Ushiyama, K.; Hozumi, A.; Takai, O. *Langmuir* **2000**, *16*, 885.
(9) Tarlov, M. J.; Burgess, D. R. F.; Gillen, G. *J. Am. Chem. Soc.* **1993**, *115*, 5305.
(10) Huang, J. Y.; Dahlgren, D. A.; Hemminger, J. C. *Langmuir* **1994**, *10*, 626.
(11) Behm, J. M.; Lykke, K. R.; Pellin, M. J.; Hemminger, J. C. *Langmuir* **1996**, *12*, 2121.
(12) Xia, Y. N.; Zhao, X. M.; Whitesides, G. M. *Microelectron. Eng.* **1996**, *32*, 255.
(13) Xia, Y. N.; Rogers, J. A.; Paul, K. E.; Whitesides, G. M. *Chem. Rev.* **1999**, *99*, 1823.
(14) Lercel, M. J.; Tiberio, R. C.; Chapman, P. F.; Craighead, H. G.; Sheen, C. W.; Parikh, A. N.; Allara, D. L. *J. Vac. Sci. Technol. B* **1993**, *11*, 2823.
(15) Yang, X. M.; Peters, R. D.; Kim, T. K.; Nealey, P. F.; Brandow, S. L.; Chen, M. S.; Shirey, L. M.; Dressick, W. J. *Langmuir* **2001**, *17*, 228.
(16) Roberson, S. V.; Fahey, A. J.; Sehgal, A.; Karim, A. *Appl. Surf. Sci.* **2002**, *200*, 150.
(17) Moise, T.; Rudich, Y. *Geophys. Res. Lett.* **2001**, *28*, 4083.
(18) Bertram, A. K.; Ivanov, A. V.; Hunter, M.; Molina, L. T.; Molina, M. J. *J. Phys. Chem. A* **2001**, *105*, 9415.
(19) Ravishankara, A. R. *Science* **1997**, *276*, 1058.
(20) Garton, D. J.; Minton, T. K.; Troya, D.; Pascual, R.; Schatz, G. C. *J. Phys. Chem. A* **2003**, *107*, 4583.
(21) Wagner, A. J.; Wolfe, G. M.; Fairbrother, D. H. *J. Chem. Phys.* **2004**, *120*, 3799.
(22) Lin, E. K.; Soles, C. L.; Goldfarb, D. L.; Trinque, B. C.; Burns, S. D.; Jones, R. L.; Lenhart, J. L.; Angelopoulos, M.; Willson, C. G.; Satija, S. K.; Wu, W. L. *Science* **2002**, *297*, 372.
(23) Atkinson, R. *J. Phys. Chem. Ref. Data* **1994**, *Monograph 1*, 1.
(24) Au, J. W.; Cooper, G.; Burton, G. R.; Olney, T. N.; Brion, C. E. *Chem. Phys.* **1993**, *173*, 209.
(25) Laibinis, P. E.; Graham, R. L.; Biebuyck, H. A.; Whitesides, G. M. *Science* **1991**, *254*, 981.
(26) Frydman, E.; Cohen, H.; Maoz, R.; Sagiv, J. *Langmuir* **1997**, *13*, 5089.

9938 *J. Phys. Chem. B, Vol. 109, No. 20, 2005*

Ye et al.

(27) Kim, T. K.; Yang, X. M.; Peters, R. D.; Sohn, B. H.; Nealey, P. F. *J. Phys. Chem. B* **2000**, *104*, 7403.

(28) Seshadri, K.; Froyd, K.; Parikh, A. N.; Allara, D. L.; Lercel, M. J.; Craighead, H. G. *J. Phys. Chem.* **1996**, *100*, 15900.

(29) Uosaki, K.; Quayum, M. E.; Nihonyanagi, S.; Kondo, T. *Langmuir* **2004**, *20*, 1207.

(30) Finlayson-Pitts, B.; Pitts, J. *Atmospheric Chemistry: Fundamentals and Experimental Techniques*; John Wiley & Sons: New York, 1986.

(31) Ferris, M. M.; Rowlen, K. L. *Appl. Spectrosc.* **2000**, *54*, 664.

(32) Lewis, M.; Tarlov, M.; Carron, K. *J. Am. Chem. Soc.* **1995**, *117*, 9574.

(33) Norrod, K. L.; Rowlen, K. L. *J. Am. Chem. Soc.* **1998**, *120*, 2656.

(34) Moon, D. W.; Kurokawa, A.; Ichimura, S.; Lee, H. W.; Jeon, I. C. *J. Vac. Sci. Technol. A* **1999**, *17*, 150.

(35) Ye, T.; Wynn, D.; Dudek, R.; Borguet, E. *Langmuir* **2001**, *17*, 4497.

(36) Sagiv, J. *J. Am. Chem. Soc.* **1980**, *102*, 92.

(37) Brzoska, J. B.; Shahidzadeh, N.; Rondelez, F. *Nature* **1992**, *360*, 719.

(38) Carraro, C.; Yauw, O. W.; Sung, M. M.; Maboudian, R. *J. Phys. Chem. B* **1998**, *102*, 4441.

(39) Horvath, M.; Bilitzky, L.; Hunttner, J. *Ozone*; Elsevier Science Publishing: New York, 1985.

(40) *Chemical Kinetics and Photochemical Data for Use in Stratospheric Modeling*; JPL Publication No. 02-251997; Jet Propulsion Laboratory, C., California Institute of Technology: Pasadena, CA, 1997.

(41) Zhukov, V.; Popova, I.; Yates, J. T., Jr. *J. Vac. Sci. Technol. A* **2000**, *18*, 992.

(42) Parikh, A. N.; Allara, D. L.; Azouz, I. B.; Rondelez, F. *J. Phys. Chem.* **1994**, *98*, 7577.

(43) Flinn, D. H.; Guzonas, D. A.; Yoon, R. H. *Colloids Surf. A* **1994**, *87*, 163.

(44) Paz, Y.; Trakhtenberg, S.; Naaman, R. *J. Phys. Chem.* **1994**, *98*, 13517.

(45) Atre, S. V.; Liedberg, B.; Allara, D. L. *Langmuir* **1995**, *11*, 3882.

(46) Stein, S. E. Infrared spectra. In *NIST Chemistry WebBook, NIST Standard Reference Database Number 69 (http://webbook.nist.gov)*; Linstrom, P. J., Mallard, W. G., Eds.; National Institute of Standards and Technology: Gaithersburg MD, 2003.

(47) Bain, C. D.; Whitesides, G. M. *J. Phys. Chem.* **1989**, *93*, 1670.

(48) Lamont, C. L. A.; Wilkes, J. *Langmuir* **1999**, *15*, 2037.

(49) Fairbank, R. W. P.; Wirth, M. J. *J. Chromatogr. A* **1999**, *830*, 285.

(50) McArthur, E.; Ye, T.; Cross, J.; Petoud, S.; Borguet, E. *J. Am. Chem. Soc.* **2004**, *126*, 2260.

(51) Apostolova, E.; Krumova, S.; Tuparev, N.; Molina, M. T.; Filipova, T.; Petkanchin, I.; Taneva, S. G. *Colloids Surf. B* **2003**, *29*, 1.

(52) Chu, S. S.; Reich, S. H. *Bioorg. Med. Chem. Lett.* **1995**, *5*, 1053.

(53) Malicka, J.; Gryczynski, I.; Gryczynski, Z.; Lakowicz, J. R. *Anal. Biochem.* **2003**, *315*, 57.

(54) Marchi-Artzner, V.; Lorz, B.; Gosse, C.; Jullien, L.; Merkel, R.; Kessler, H.; Sackmann, E. *Langmuir* **2003**, *19*, 835.

(55) Singh, Y.; Gulyani, A.; Bhattacharya, S. *FEBS Lett.* **2003**, *541*, 132.

(56) Hayashi, Y.; Ichimura, K. *J. Fluoresc.* **2003**, *13*, 129.

(57) Herold, M.; Brunner, H.; Tovar, G. E. M. *Macromol. Chem. Phys.* **2003**, *204*, 770.

(58) Lee, K. B.; Yoon, K. R.; Woo, S. I.; Choi, I. S. *J. Pharm. Sci.* **2003**, *92*, 933.

(59) Wang, W. L.; He, Q. G.; Zhai, J.; Yang, J. L.; Bai, F. L. *Polym. Adv. Technol.* **2003**, *14*, 341.

(60) Fox, M. A.; Li, W. J.; Wooten, M.; McKerrow, A.; Whitesell, J. K. *Thin Solid Films* **1998**, *329*, 477.

(61) Montalti, M.; Prodi, L.; Zaccheroni, N.; Baxter, R.; Teobaldi, G.; Zerbetto, F. *Langmuir* **2003**, *19*, 5172.

(62) Flink, S.; van Veggel, F. C. J. M.; Reinhoudt, D. N. *J. Phys. Org. Chem.* **2001**, *14*, 407.

(63) Brown, W. *Introduction to Organic Chemistry*; Willard Grant Press: Boston, 1982.

(64) Zahr, G. E.; Preston, R. K.; Miller, W. H. *J. Chem. Phys.* **1975**, *62*, 1127.

(65) Atkins, P.; Paula, J. *Physical Chemistry*, 7th ed.; W. H. Freeman and Company: New York, 2002.

(66) Tevault, D. E.; Mowery, R. L.; Smardzewski, R. R. *J. Chem. Phys.* **1981**, *74*, 4480.

(67) Colvin, E. W. *Silicon in Organic Synthesis*; Robert E Krieger Publishing Co.: Malabar, FL, 1985.

(68) Israelachvili, J. N.; Gee, M. L. *Langmuir* **1989**, *5*, 288.

(69) Bain, C. D.; Whitesides, G. M. *Science* **1988**, *240*, 62.

(70) Cox, R.; Patrick, K.; Chant, S. *Environ. Sci. Technol.* **1981**, *15*, 587.

(71) Martinez, R. D.; Buitrago, A. A.; Howell, N. W.; Hearn, C. H.; Joens, J. A. *Atmos. Environ. Part A* **1992**, *26*, 785.

(72) Maricq, M. M.; Wallington, T. J. *J. Phys. Chem.* **1992**, *96*, 986.